


Article

Beta Decay in Medium-Mass Nuclei with the In-Medium Similarity Renormalization Group

Steven Ragnar Stroberg 

Physics Division, Argonne National Laboratory, Lemont, IL 60439, USA; sstroberg@anl.gov

Abstract: We review the status of ab initio calculations of allowed beta decays (both Fermi and Gamow–Teller), within the framework of the valence-space in-medium similarity renormalization group approach.

Keywords: ab initio; Gamow–Teller beta decay; superallowed Fermi decays



Citation: Stroberg, S.R. Beta Decay in Medium-Mass Nuclei with the In-Medium Similarity Renormalization Group. *Particles* **2021**, *4*, 521–535. <https://doi.org/10.3390/particles4040038>

Academic Editor: Stefano Gandolfi, Vincenzo Cirigliano and Emanuele Mereghetti

Received: 6 September 2021

Accepted: 27 October 2021

Published: 18 November 2021

Publisher's Note: MDPI stays neutral with regard to jurisdictional claims in published maps and institutional affiliations.



Copyright: © 2021 by the author. Licensee MDPI, Basel, Switzerland. This article is an open access article distributed under the terms and conditions of the Creative Commons Attribution (CC BY) license (<https://creativecommons.org/licenses/by/4.0/>).

1. Introduction

Beta decays in atomic nuclei have long been a source of fundamental discoveries in physics [1–3], and precise measurements of beta decays continue to be a promising path to search for physics beyond the Standard Model (BSM) [4–7]. A major challenge in the search for a signal of new physics is understanding the Standard Model “background”, especially the effects of low-energy quantum chromodynamics which manifest as nuclear structure. The situation is aggravated by the fact that nuclei which are preferred experimentally are often difficult to treat theoretically in a framework that allows quantified uncertainties.

Nevertheless, progress has been made over the past few decades so that the inter-nucleon interaction can be systematically constructed within an effective field theory framework [8–10]. Simultaneously, advances in many-body theory and computational resources have enabled ab initio treatment of the medium-mass nuclei which are often relevant for BSM searches [11–17]. Of course, more work remains to be done, both on the effective field theory side [18–20] and on understanding how approximation schemes in ab initio calculations impact the observables in question.

In this paper, I will focus on one particular many-body method—the valence-space in-medium similarity renormalization group (VS-IMSRG)—and consider two topics in allowed beta decay, the quenching in Gamow–Teller decays and correction factors for superallowed $0^+ \rightarrow 0^+$ Fermi decays.

2. IMSRG Formalism

There are several review articles detailing both the free-space SRG [21,22] and the in-medium SRG [15,23–26], and so here I will review only what is needed for our present purposes.

2.1. Similarity Renormalization Group

The basic idea of the SRG is to perform a unitary transformation U on the Hamiltonian H (and all other operators) in such a way that the resulting nuclear wave function is simpler. This is achieved by performing a sequence of infinitesimal unitary transformations, labeled by a flow parameter s , so that

$$H(s) = U(s)H(0)U^\dagger(s) \quad (1)$$

with $U(0) = 1$. The way in which U changes with s is specified by the action of an operator η , called the generator:

$$\frac{dU(s)}{ds} = \eta(s)U(s). \quad (2)$$

We are free to choose η however we like—it can depend on s —as long as it is anti-hermitian, i.e., $\eta^\dagger(s) = -\eta(s)$. Combining (1) and (2) we obtain a flow equation for the Hamiltonian in terms of a commutator with the generator

$$\frac{dH}{ds} = [\eta(s), H(s)]. \quad (3)$$

The flow equation for any other operator \mathcal{O} is obtained by replacing $H \rightarrow \mathcal{O}$ on both sides of (3) [27–30].

It remains to specify $\eta(s)$. In the free-space SRG, we choose

$$\eta^{SRG}(s) = [T, V(s)] \quad (4)$$

where T is the kinetic energy and $V(s)$ is the potential so $H(s) = T + V(s)$. This generator drives $V(s)$ towards a band-diagonal form in momentum space, with a width $\lambda_{SRG} \equiv s^{-1/4}$.

When the SRG flow Equation (3) is formulated in Fock-space (i.e., in terms of creation and annihilation operators), many-body forces are inevitably induced, and these must be truncated in order to make the calculation tractable. For this reason, the “free-space” SRG evolution is typically performed out to $\lambda_{SRG} \gtrsim 2 \text{ fm}^{-1}$.

2.2. In-Medium SRG

The truncation of many-body forces is rendered less severe if all operators are normal-ordered with respect to a reference state $|\Phi\rangle$, which should be a reasonable first approximation of the exact wave function $|\Psi\rangle$. This approach is called the in-medium SRG (IMSRG). If we choose the generator to suppress the parts of H which lead to excitations out of the reference $|\Phi\rangle$, then for $s \rightarrow \infty$ $|\Phi\rangle$ becomes an eigenstate of $H(s)$ with an eigenvalue corresponding to the energy of the exact wave function $|\Psi\rangle$, up to approximation errors in solving (3). In all calculations presented here, I neglect three-body operators after the initial normal-ordering step, resulting in the IMSRG(2) approximation.

One possible choice for the generator which achieves the desired suppression was proposed by White [31]

$$\langle a|\eta^{Wh}|b\rangle \equiv \frac{\langle a|H^{od}|b\rangle}{E_a - E_b} \quad (5)$$

where the “off-diagonal” part of the Hamiltonian, denoted H^{od} , is any part of H which connects $|\Phi\rangle$ to a different state. The states $|a\rangle$ and $|b\rangle$ are elements of the basis used to express the operators, and the denominator $E_a - E_b$ is the energy difference between the basis states. (The denominators are typically defined with Epstein–Nesbet or Møller–Plesset partitioning. In this work, I use Epstein–Nesbet denominators, and a modification of (5)—also suggested by White—called the arctangent generator (see Ref. [26] for more details).)

As a further generalization, we may define a valence space (e.g., the sd-shell above an ^{16}O core), and define H^{od} as any part of H which connects a valence configuration to a non-valence configuration (specifically, we partition all single-particle states into core, valence, and excluded orbits. A “valence configuration” is one with all core orbits occupied and all excluded orbits unoccupied). The Hamiltonian is then driven to a block-diagonal form and we may diagonalize in the (typically much smaller) sub-space of valence configurations. Such a diagonalization directly corresponds to a standard large-scale shell model calculation with an effective interaction defined by $H(\infty)$. This approach is referred to as the valence-space IMSRG (VS-IMSRG), and it is used for all calculations presented.

Generally, the states we wish to target in a valence space approach are not well-described by a single closed-shell configuration, and the choice of $|\Phi\rangle$ becomes less clear. In this work I use the ensemble normal-ordering (ENO) approach [32], which amounts to taking fractional occupation numbers such that the reference has spherical symmetry and

the correct number of particles on average. In addition, I use the Magnus formulation of the IMSRG [33], in which we write

$$U(s) \equiv e^{\Omega(s)} \quad (6)$$

where $\Omega = -\Omega^\dagger$ is the Magnus operator. Equations (6) and (2) may be combined to obtain a flow equation for $\Omega(s)$ in terms of $\eta(s)$, and operators (including the Hamiltonian), are transformed as

$$\begin{aligned} \mathcal{O}(s) &= e^{\Omega(s)} \mathcal{O}(0) e^{-\Omega(s)} \\ &= \mathcal{O}(0) + [\Omega(s), \mathcal{O}(0)] + \frac{1}{2!} [\Omega(s), [\Omega(s), \mathcal{O}(0)]] + \dots \end{aligned} \quad (7)$$

In (7), each commutator is truncated at the normal-ordered two-body level, and the series is computed iteratively until the size of a term falls below a numerical threshold.

2.3. Aspects Relevant to Beta Decay

Two additional details of the calculation are relevant for β decays. The first is the choice of single-particle basis in which we express the operators at $s = 0$. In this work I use a Hartree–Fock basis with Coulomb and isospin-breaking strong forces included, so that for a given set of single-particle quantum numbers $\{n, \ell, j\}$, the proton and neutron radial wave functions are not identical. The second is the choice of reference. Because we wish to compute the initial state, with N neutrons and Z protons, consistently with the final state with $N \pm 1$ neutrons and $Z \mp 1$ protons, there is some ambiguity about which reference $|\Phi\rangle$ should be used. If we retain all induced many-body terms during the SRG evolution, the choice of reference is irrelevant. However, the accuracy of the IMSRG(2) approximation depends on the choice of reference. The two natural choices for β decay are to use the N, Z of the initial state or the final state. I will discuss this in more detail in Section 4.

2.4. Comparison with Other Ab Initio Methods

Besides the VS-IMSRG, there are a number of ab initio methods available which can be used to treat beta decay, and it is worth briefly outlining them for context. For a more detailed account of ab initio many-body methods for nuclei, the reader is referred to [15]. Quantum Monte Carlo [11] and no-core shell model [34] approaches have well-understood approximation errors and can often yield quasi-exact solutions. The price is that the computational cost of these methods scales exponentially with the number of particles, and so are generally limited to the p -shell, with $A \lesssim 16$.

Polynomially-scaling methods, like coupled cluster (CC) [12], self-consistent Green's function [35], IMSRG [23], and many-body perturbation theory (MBPT) [36], can access heavier nuclei at the cost of approximation errors that, while systematically improvable, are more difficult to assess. With the exception of quantum Monte Carlo (which requires a local potential), all of these methods can use the same input Hamiltonian and operators, enabling benchmark comparisons to better understand many-body errors [37,38].

Perhaps the most significant difference between the VS-IMSRG approach and the other polynomially-scaling methods is that the latter methods are generally constructed to target a single (ground) state of a given nucleus, and other states are expressed in terms of particle-hole excitations out of that state (notable exceptions being the shell model couple- cluster approach [39], which decouples a valence space in a similar manner to the VS-IMSRG, and the in-medium generator coordinate method [40] in which initial and final states are expressed by superpositions of shapes). This can in principle lead to trouble for transitions between states which are not, to a good approximation, related by a few particle-hole excitations. In contrast, the VS-IMSRG, by virtue of an exact diagonalization in the valence space, can describe two states which are related by many-particle-many-hole excitations—so long as those excitations live in the valence space.

It bears emphasis that all the above methods are systematically improvable and, given the same input Hamiltonian, should all converge to the same answer as their respective

truncations are relaxed. Which truncation scheme converges most rapidly will in general depend on the state and observable in question. Consequently, until the truncation errors of polynomial-scaling methods are more quantitatively understood, benchmarks and cross-checks between methods are essential for making robust predictions.

3. Gamow–Teller Decays

In a Gamow–Teller decay, the leptons carry one unit of angular momentum and leave the parity of the nucleus unchanged. The relevant nuclear transition operator is obtained from the space-like part of the hadronic axial-vector current. The leading term in the non-relativistic reduction is $g_A \sigma \tau$, where $g_A \approx 1.27$ is the axial coupling constant, and σ and τ are the spin and isospin Pauli matrices.

Historically, when the leading operator was combined with shell model wave functions, a systematic “quenching” of the decay strength was observed, i.e., experimental matrix elements were smaller than the predicted ones, with a similar effect (it should be noted that the quenching in $M1$ observables is less clear experimentally, see e.g., Ref. [41]. Two body currents have been shown to improve agreement with experiment in quantum Monte Carlo calculations of p -shell nuclei [42], but these currents have not yet been studied in ab initio calculations of heavier systems) in isovector $M1$ observables [43–48]. It was quickly surmised that the source of the discrepancy should be some combination of inadequate wave functions (missing correlations) and an inadequate transition operator (missing currents), that neither of these obviously dominated and that the two effects were not independent [44,49,50]. It was also suggested that pions ought to have something to do with the renormalization of the axial current in the nuclear medium [51].

These physics arguments survive in the modern EFT point of view, which organizes the nuclear interaction and coupling to external fields in powers of a ratio of scales. The distinction between short and long-distance physics is made by a cutoff, and the arbitrariness of the cutoff is reflected in the requirement that observables be independent of its value. The relationship between pions and the axial current arises as a consequence of broken chiral symmetry [52]. Importantly, chiral EFT enables a systematic and consistent construction of three-nucleon forces and two-body currents [53–56].

The result in the limit that the momentum carried by the leptons vanishes, up to order Q^0 (leading order is Q^{-3}) is [53,57,58]

$$\vec{J} = \vec{J}_{1b} + \vec{J}_{2b;\text{cont}} + \vec{J}_{2b;1\pi} \quad (8)$$

where

$$\vec{J}_{1b}^{\pm} = g_A \vec{\sigma} \tau^{\pm} \quad (9)$$

$$\vec{J}_{2b;\text{cont}}^{\pm} = \frac{1}{2} \frac{c_D}{\Lambda_{\chi} f_{\pi}^2} (\vec{\sigma}_1 \tau_1^{\pm} + \vec{\sigma}_2 \tau_2^{\pm}) \quad (10)$$

$$\vec{J}_{2b;1\pi} = -\frac{g_A}{f_{\pi}^2} \frac{\vec{\sigma}_2 \cdot \vec{q}_2}{k_2^2 + M_{\pi}^2} \left[\frac{i \vec{p}_1}{2m} \tau_{\times}^{\pm} + 2c_3 \tau_2^{\pm} \vec{k}_2 + (c_4 + \frac{1}{4m}) \tau_{\times}^{\pm} (\vec{\sigma}_1 \times \vec{k}_2) \right] + (1 \leftrightarrow 2) \quad (11)$$

where \vec{p}_i, \vec{p}'_i are the incoming and outgoing momenta of the i th nucleon, $\vec{k}_i = \vec{p}'_i - \vec{p}_i$, $\tau_{\times} = \tau_1 \times \tau_2$, and f_{π} is the pion decay constant. The low-energy constants c_3, c_4 and c_D also enter into the NN and 3N forces, and so are not additional free parameters. (The constant c_D is dimensionless and expected to be $O(1)$, while c_i ($i = 3, 4$) have mass dimension -1 . The dimensionless quantities $\hat{c}_i \equiv m_N c_i$ are expected to be $O(1)$.) Equations (9)–(11) correspond to diagrams (a), (b), and (c) in Figure 1, respectively. There are also corrections to the one-body operator of order p_i^2/m_N^2 . Depending on how the nucleon mass is counted, these corrections will enter at different orders. In the counting of e.g., Park et al. [53], these corrections are also Q^0 , while in the counting used by other authors [37,56,58], including the calculations in this paper, these corrections are Q^1 . It is also worth noting that, because terms of order Q^{-2} vanish, some authors label Q^{-1} terms as next-to-leading-

order (NLO) [56], while others call this next-to-next-to-leading-order (NNLO) [53]. To avoid confusion, I shall explicitly refer to powers of Q .

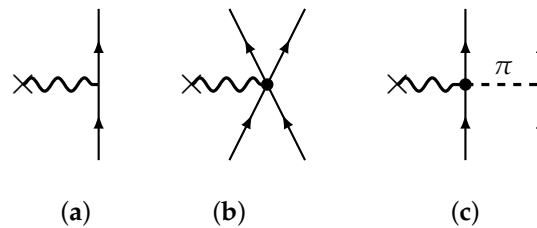


Figure 1. Diagrams for (a) leading-order Gamow–Teller decay $\sigma\tau$, (b) short-range two-body current, and (c) long-range two-body current.

In Refs. [57,58], these currents were normal ordered with respect to uniform nuclear matter to obtain an in-medium quenching factor for the one-body operator. In Ref. [59], the full two-body current was constructed, consistently (in [59], the relationship between the two-body currents and three-body force contained an erroneous factor of $-1/4$ [55]) with the NN + 3N force, and the normal-ordered one-body operator (with respect to a Hartree–Fock reference) was used to compute Gamow–Teller decays of ^{14}C , ^{22}O , and ^{24}O with the coupled-cluster method. (I also note that while the decay of ^{14}C is interesting due to the anomalously long half-life [60,61], the small matrix element makes it difficult to draw conclusions regarding systematic quenching effects.) The effect of the residual normal-ordered two-body part of the operator was estimated and found to be small. In all three of these cases, a quenching of about the right size was obtained. In Ref. [62], axial currents up to Q^1 were used in quantum Monte Carlo calculations of $A = 6$ – 10 nuclei, where it was found that correlations beyond the shell model accounted for most of the quenching, with subleading currents playing a minor role. In Ref. [37], the full two-body current up to Q^0 was constructed consistently with the NN + 3N force, consistently SRG evolved, and evaluated, with the normal-ordered two-body operator fully included, in a range of nuclei in the p , sd , and pf shells, as well as ^{100}Sn , using no-core shell model, coupled cluster, or VS-IMSRG to solve the many-body problem. Here, I will provide some additional calculations not presented in [37], and some further discussion. Specifically, I use an interaction for which no VS-IMSRG results were presented in [37] (though the conclusions drawn are the same), and I select additional transitions with large matrix elements to better emphasize the quenching “signal” over valence-space configuration-mixing “noise”.

The experimental Gamow–Teller matrix elements are obtained from the ft values by

$$ft = \frac{K}{\left[\frac{f_V}{f_A} B(F) + B(GT) \right] G_V^2} \quad (12)$$

with $K \equiv (2\pi^3 \hbar^7 \ln 2) / (m_e^5 c^4)$, and $K/G_V^2 \approx 6140$ s. The Gamow–Teller matrix element is defined as

$$M(GT) \equiv [(2J_i + 1)B(GT)]^{1/2}. \quad (13)$$

Note different definitions have been used in the literature, e.g., one may divide the right hand side by g_A , as was done in [37]. The definition (13) leaves the experimental value independent of the adopted form of the current, or the adopted value of g_A . The theoretical matrix element is given by $M_{GT} = \langle \Psi_f || \vec{J} || \Psi_i \rangle$, with the current \vec{J} as defined in (8), with or without the two-body part.

I consider Gamow–Teller transitions in nuclei in the p , sd , and pf shells, with experimental data taken from Refs. [46–48]. I have selected transitions with large transition matrix elements, with the goal of reducing sensitivity to fine-tuned cancellations. I also consider the decay of ^{100}Sn , which was treated with equations-of-motion coupled cluster in [37], and for which the experimental picture is still somewhat conflicted [63–66]. I adopt the average value presented in [66]. In the VS-IMSRG calculation of ^{100}Sn , I use valence

space consisting of the $0f_5, 1p_3, 1p_3, 0g_9$ orbits for protons and $0f_7, 1d_5, 1d_3, 2s_1, 0h_{11}$ for neutrons.

For the theoretical calculations, I use the NN + 3N (lnl) interaction developed by Navrátil [35]. The interaction and current are consistently SRG-evolved to a scale $\lambda_{\text{SRG}} = 2.0 \text{ fm}^{-1}$ and evaluated in an oscillator space defined by $2n + \ell \leq e_{\text{max}} = 12$ and $\hbar\omega = 16$. The 3N matrix elements are further truncated with $e_1 + e_2 + e_3 \leq E_{3\text{max}} = 14$. All operators are transformed to the Hartree–Fock basis, and then the residual 3N operators are truncated (the NO2B approximation). Next, a VS-IMSRG calculation is performed using the code `imsrg++` [67], yielding an effective valence space interaction and operator. The valence space diagonalization is carried out either using `NuShellX@MSU` [68] with operators evaluating using the code `nutbar` [69], or with `KSHELL` [70]. The results are listed in Table A1 and plotted in Figure 2.

Table A1 in the appendix contains the numerical results. The column labeled $M(GT)_{\text{exp}}$ lists the experimental Gamow–Teller matrix elements defined by (13) (experimental uncertainties are not listed). The column labeled $\sigma\tau_{\text{bare}}$ is the obtained by evaluating the operator $\sigma\tau$ (assuming identical radial wave functions for protons and neutrons) between valence space wave functions obtained using the VS-IMSRG evolved interaction. The column labeled $\sigma\tau_{\text{IMSRG}}$ is obtained by consistently SRG and VS-IMSRG evolving the $\sigma\tau$ operator (including the radial mismatch due to the Hartree–Fock basis). Finally, $M(GT)_{\text{th}}$ also includes the two-body currents, consistently SRG and VS-IMSRG evolved. In a few cases, the listed strength is summed over multiple final states with the same spin and parity.

In Figure 2, panel (a) shows a scatter plot of $M(GT)_{\text{exp}}$ vs $M(GT)_{\text{bare}}$, while panel (b) shows $M(GT)_{\text{th}}$ vs $M(GT)_{\text{exp}}$. The solid line shows $y = x$ corresponding to the perfect agreement between theory and experiment. The dashed line shows a best-fit slope, which is indicated as a quenching factor at the top of the figure. For this quenching factor, I only include *sd* and *pf* shell nuclei because the *p* shell nuclei have a large scatter due to nuclear structure details. The quantity in parenthesis indicates the standard deviation about the best-fit line. If I include *p* shell nuclei in the fit, the full theory quenching factor changes to $q = 0.99$, but the standard deviation increases to 0.21.

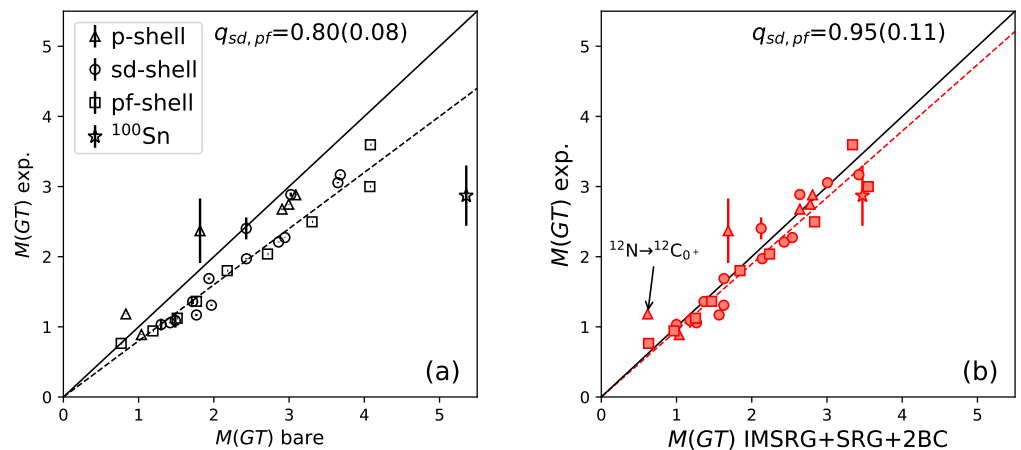


Figure 2. Experimental $M(GT)$ vs. $M(GT)$ obtained with (a) the bare $g_A\sigma\tau$ operator, (b) the SRG- and IMSRG-transformed transition operator including two-body currents. In both panels, the solid line shows $y = x$ corresponding to perfect agreement, while the dashed line indicates the best-fit slope.

It is evident from Table A1 that both the correlations included in $\sigma\tau_{\text{IMSRG}}$ and the two-body currents lead to a reduction of the Gamow–Teller matrix element. As discussed in Ref. [37], the detailed breakdown of the quenching into correlations and currents is scheme- and scale-dependent; some of the effects attributed to correlations when using a hard interaction get shuffled into currents, when using a soft interaction. Thus the smaller impact of currents found in quantum Monte Carlo calculations [62] is consistent with the

harder interactions used. However, even with soft interactions, the impact of currents for p -shell nuclei is less than for heavier systems.

It is also evident from Figure 2 that the systematic quenching effect, observed when using the bare $\sigma\tau$ operator, essentially vanishes when using the consistently-evolved operator including two-body currents.

In the right panel of Figure 2 I highlight the transition $^{12}\text{N} \rightarrow ^{12}\text{C}_{0+}$ as an illustration of the cancellation effects in the p shell which wash out the quenching signal. When evaluating the bare $\sigma\tau$ operator (the matrix element of the bare operator is not an observable, so strictly there's no reason different Hamiltonians should agree on it. On the other hand one might expect some degree of universality within a low-resolution picture like the shell model [21,71]) (including g_A), there are four terms that contribute, corresponding to proton-to-neutron transitions $p_3 \rightarrow p_3$, $p_3 \rightarrow p_1$, $p_1 \rightarrow p_3$, and $p_1 \rightarrow p_1$. The contributions are +0.366, −0.955, +1.592, and −0.173, respectively, totaling to 0.830. Evidently, there is significant cancellation so that a relatively small change of the individual terms can lead to a relatively large change on the final matrix element. For example, if I use valence-space wave functions obtained with the phenomenological Cohen–Kurath interaction [72], the bare operator yields a matrix element of 1.219. This difference, due to configuration mixing within the valence space, is larger than the systematic quenching effect of interest.

We may view this “noise” in the quenching from another perspective. Figure 3 shows the theory-to-theory quenching factor $M(GT)_{\text{th}}/M(GT)_{\text{bare}}$ as a function of mass number. This indicates the quenching factor needed if we wanted to approximately account for the correlations and currents contained in $M(GT)_{\text{th}}$. The main point here is to emphasize that the quenching is not a smooth function of A , but in fact has considerable state dependence.

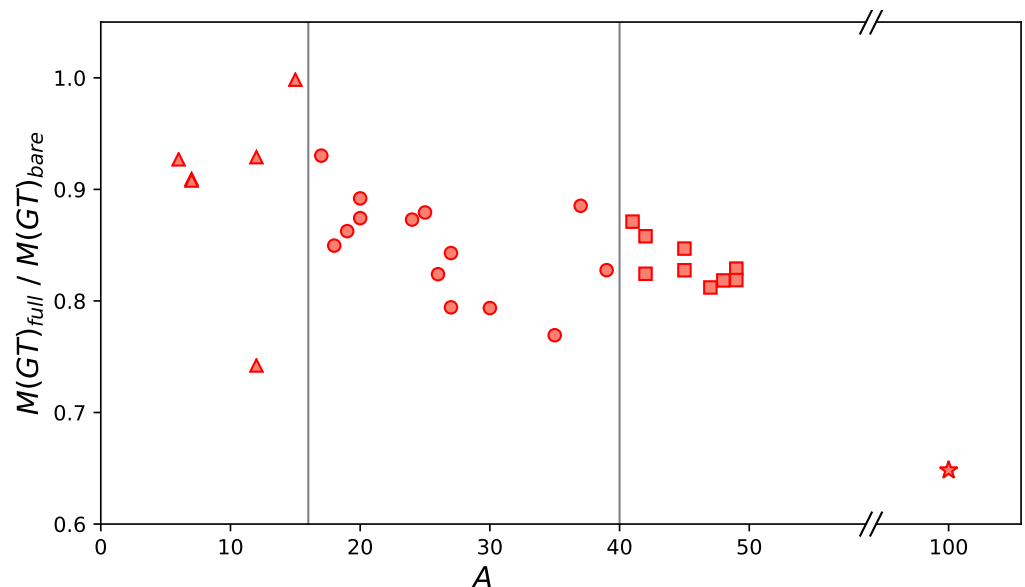


Figure 3. Theory-to-theory “quenching” factors as a function of mass number A .

It is clear that including two-body currents consistently with the $\text{NN} + 3\text{N}$ interaction helps to remove the ambiguity of empirical quenching factors. Moving forward, the analogous calculation should be pursued for double beta decay, where the quenching effect is an important source of uncertainty [58,73]. In single beta decay, it will be important to explore the impacts of currents from the next order in the chiral expansion to confirm the convergence.

4. Superaligned $0^+ \rightarrow 0^+$ Fermi Decays

For transitions between $J = 0$ states, $B(GT) = 0$ by conservation of angular momentum. Furthermore, in the limit in which isospin is a perfect symmetry, a “superaligned” transition between $T = 1$ isobaric analogue states yields $B(F) = 2$, and so (12) reduces to (I am also neglecting here radiative corrections, which have a non-negligible impact)

$$ft = \frac{K}{2G_V^2} \quad (\text{isospin limit}) \quad (14)$$

(where here $f = f_V$). This implies all superaligned $0^+ \rightarrow 0^+$ should have the same ft value, and that from this one may measure the coupling constant for semileptonic decay G_V , which is in turn related to the constant G_F obtained from muon decay by $G_V = V_{ud}G_F$, where V_{ud} is the up-down element of the Cabibbo–Kobayashi–Maskawa (CKM) quark mixing matrix. Consequently, precise ft measurements of superaligned $0^+ \rightarrow 0^+$ decays provide a sensitive test of the Standard Model: non-universality of superaligned ft values, or non-unitarity of the CKM matrix would be signs of new physics.

Of course, isospin is not a perfect symmetry of the Standard Model. It is broken by the quark electric charges, and the up-down mass difference. This is manifested at the nuclear level as the Coulomb force between protons and isospin-violating strong interactions. The Standard Model corrections to (14) have been parameterized by Towner and Hardy [6] as

$$\mathcal{F}t \equiv ft(1 + \delta'_R)(1 + \delta_{NS} - \delta_C) = \frac{K}{2G_V^2\Delta_R^V}. \quad (15)$$

In (15) Δ_R^V is a process-independent radiative correction [74], δ'_R is a radiative correction only depending on the electron energy and the charge of the daughter nucleus, and δ_{NS} is a radiative correction depending on the detailed nuclear structure. The isospin-symmetry-breaking correction δ_C accounts for the fact that the final state is not exactly an isospin rotation of the initial state.

Consequently, only δ_{NS} and δ_C are the purview of nuclear structure theory. To draw an analogy with the situation for Gamow–Teller decays, δ_C corresponds to including the effects of correlations for the leading operator τ , while the radiative corrections correspond to sub-leading corrections to the operator, with δ_{NS} corresponding to two-body currents. The difference here is that the corrections are sub-leading in the fine structure constant $\alpha \approx 1/137$ (or $Z\alpha$), as opposed to the chiral EFT expansion parameter $Q \sim 1/4$. The various corrections are illustrated in Figure 4.

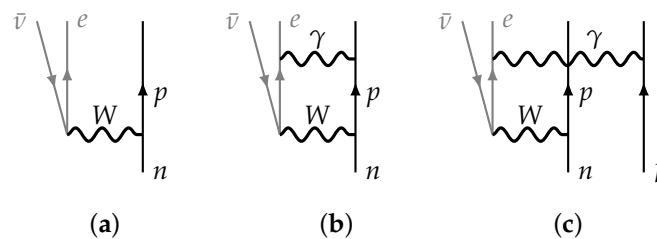


Figure 4. Schematic high-resolution diagrams corresponding to (a) the leading operator τ , (b) the one-body correction leading to Δ_R^V and δ'_R , and (c) the two-body correction leading to δ_{NS} .

In this paper, we focus on the δ_C correction, for no better reason than the operator is the simplest to implement. Towner and Hardy decompose δ_C into a correction due to isospin-breaking configuration mixing effects, and a correction due to the mismatch in single-particle wave functions between protons and neutrons. As we will be treating both within a consistent calculation, such a decomposition is not necessary (and ambiguous) and we will simply use

$$\delta_C = 1 - |M_F|^2/2 \quad (16)$$

where $M_F = \langle \Psi_f | \tau | \Psi_i \rangle$ is the result of the ab initio calculation.

Nevertheless, it is useful to keep the two mechanisms (configuration mixing and wave function mismatch) in mind when considering the impact of various approximations. The wave function mismatch effect is taken into account primarily by the fact that we use a Hartree–Fock single-particle basis, with Coulomb and nuclear ISB effects included in the potential (see also [75]).

To get an idea of what the VS-IMSRG framework produces for the isospin-breaking correction δ_C , I consider three transitions spanning the p , sd , and fp shells: $^{14}\text{O} \rightarrow ^{14}\text{N}$, $^{34}\text{Ar} \rightarrow ^{34}\text{Cl}$, and $^{46}\text{Cr} \rightarrow ^{46}\text{V}$. I take the 1.8/2.0 (EM) interaction [76] with oscillator frequency $\hbar\omega = 16$ MeV and $E_{3\text{max}} = 16$. The resulting δ_C values are plotted in Figure 5 as a function of the e_{max} truncation. I show results where the normal-ordering reference $|\Phi\rangle$ is taken to be either the initial or the final nucleus, and also the results from including only the one-body part of the evolved operator. For reference, I also indicate the δ_C values adopted by Towner and Hardy [6].

If the calculation were under control, we should observe the following: convergence with respect to e_{max} ; independence of the choice of reference; and a relatively small correction from including induced two-body terms, indicating a converging hierarchy of the cluster expansion. For the $^{46}\text{Cr} \rightarrow ^{46}\text{V}$ transition, we observe reference independence and a small two-body correction, but only a hint of convergence in e_{max} . For the lighter nuclei, the situation is worse, especially for $^{14}\text{O} \rightarrow ^{14}\text{N}$. In all cases, it appears that the large e_{max} behavior will need to be incorporated in some manner, possibly by utilizing natural orbitals [77,78], or by obtaining an extrapolation formula [79,80]. However, I leave this for future work. It appears that, at least for the near term, such calculations will tell us more about the IMSRG than about physics beyond the Standard Model.

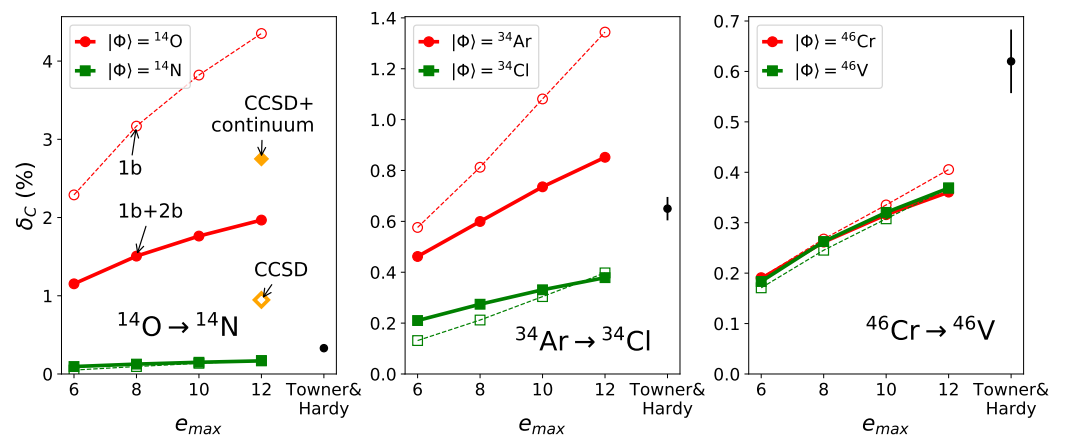


Figure 5. Isospin-breaking correction δ_C for three transitions, computed with the VS-IMSRG as a function of the e_{max} truncation. Dashed lines show the result using only the one-body part of the evolved operator while solid lines also include induced two-body terms. The black circles indicate the preferred values reported by Towner and Hardy [6]. For the ^{14}O decay, we also include coupled-cluster points [81].

The transition $^{14}\text{O} \rightarrow ^{14}\text{N}$ warrants a closer inspection, because it is light enough that it can be benchmarked against the no core shell model [34], although the observed e_{max} dependence suggests converged results may be challenging. Moreover, the dramatic reference-dependence and contribution of two-body terms make this a good system for studying such effects, which are also important (in double beta decay, the bare operator is already two-body, and we are concerned with induced three-body terms, making this a more challenging case) in neutrinoless double beta decay [38,73,82,83]. The two references used are shown schematically in Figure 6.

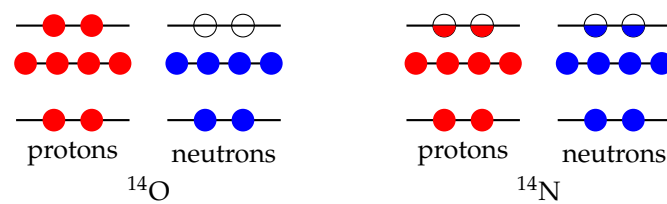


Figure 6. Schematic illustration of reference states used for the $^{14}\text{O} \rightarrow ^{14}\text{N}$ decay in the left panel of Figure 5. The half-filled circles for ^{14}N indicate the equal filling of m -states used in the ensemble reference.

Because ^{14}O is a closed shell, it may also be treated by the coupled-cluster method [12] with the transition handled by the isospin-breaking equation-of-motion approach [59]. The strong e_{max} dependence suggests sensitivity to infrared physics, and this may be probed by including the continuum in the coupled-cluster calculation [84]. The results at $e_{\text{max}} = 12$ are indicated with yellow diamonds in Figure 5. The large δ_C correction obtained with coupled cluster, as well as the substantial effect of including the continuum reinforces the notion that the pathology is not unique to the IMSRG.

The reference dependence persists even down to $e_{\text{max}} = 3$, which is sufficiently small that we may directly perform truncated configuration interaction (CI) calculations and extrapolate to the full CI result. At $e_{\text{max}} = 3$, the VS-IMSRG yields δ_C values of 0.839% and 0.056% with ^{14}O and ^{14}N references, respectively. The full CI result is 0.081%, which is considerably closer to the ^{14}N reference value. This reinforces our suspicion that the calculation with the ^{14}O reference is misbehaving.

As I mentioned above, results would be independent of the reference if all induced many-body terms were retained during the IMSRG evolution. In practice, we only retain up to two-body operators, so any reference dependence indicates the impact of discarded three-body or (if we are especially unlucky) higher-body terms. If I truncate the expansion (7) for the transformed operator at two nested commutators, the reference dependence remains, while truncating at one nested commutator eliminates the effect. This suggests that three-body operators—which first show up at two nested commutators if $\mathcal{O}(0)$ is purely one-body—are the culprit.

A more complete investigation would benefit from calculations at the IMSRG(3) level, which are becoming available [85], but which will not be pursued here. For the moment, I will speculate. It appears that using the ^{14}O reference produces the largest error on the δ_C value out of all the calculations presented in Figure 5. This is naively counterintuitive because ^{14}O is a closed shell and should be best approximated by the single-configuration reference. However, we are interested in the extent to which isospin symmetry is violated. Choosing a reference that approximates ^{14}O well but does a poor job for ^{14}N artificially breaks this symmetry, leading to an overestimate of the correction δ_C . On the other hand, the ensemble ^{14}N reference used is not a great approximation of the state of interest in ^{14}N , which is actually open shell. Using the ^{14}N ensemble reference, we make an error in our description of ^{14}N , and we make a similar error in the description of ^{14}O , so the artificial breaking of isospin symmetry is reduced. In support of this, using a ^{12}C reference, which is a poor approximation of both ^{14}O and ^{14}N , results in δ_C values in very close agreement to those obtained with the ^{14}N reference.

This is in line with the behavior observed with other relative quantities, namely excitation energies and separation energies. It is a robust finding that the VS-IMSRG predicts too-high 2^+ excitation energies for closed-shell nuclei [86,87]. This can be understood by considering that the reference is a good approximation of the 0^+ ground state, and a worse approximation for the 2^+ excited state. The truncation of three-body terms has a more severe impact on the 2^+ state, leading to missed correlation energy, and consequently an excitation energy that is too high. For open-shell nuclei, the reference is a mediocre approximation of both the ground and excited states, and so they are treated on more equal footing, leading to a more accurate excitation energy. Likewise, it was observed that separation energies are more accurately obtained when using the same valence space for

both the mass A and mass $A - 1$ nuclei, even if a different valence space might produce a more accurate ground state for one of the nuclei [88].

Preliminary studies have found that including three-body terms ameliorates the issue with 2^+ states, and an analogous effect is observed in coupled cluster [89]. Presumably retaining three-body terms would also reduce the dependence of separation energies on the choice of valence space, but this has not yet been explored. One hopes that then including three-body terms will also help with the δ_C calculation.

5. Conclusions and Outlook

We are in an exciting time in nuclear structure theory, in which it is becoming possible to address issues that were long plagued by ambiguities arising from inconsistent modeling. On the question of Gamow–Teller decays, considerable progress has been made and it appears the issue is understood. However, in order to fully put the question to rest one should properly assess theoretical errors from the EFT truncation and the many-body solution, and demonstrate systematic improvement in both.

In addition, a similar quenching is observed in strong-interaction charge exchange reactions [90], where it is assumed that the transition operator for the target nucleus is proportional to $\sigma\tau$. The quenching is often ascribed to missing strength at higher energies (the equivalent of “correlations” in beta decay). However, three-body forces should play an analogous role as two-body currents do for beta decay (replace the axial current in the diagrams in Figure 1 with an additional nucleon). From another point of view, the three-body forces correspond to an effective density-dependent two-nucleon interaction, which has also been considered in this context [91]. In practice, charge exchange cross sections are often analyzed by normalizing to a low-lying beta decay transition [92], thus implicitly assuming that any quenching effects in charge exchange scale identically to those in beta decay. It will be interesting to quantitatively investigate this parallel.

For superallowed Fermi decays, the work of Towner and Hardy [6] has laid a clear path, but there is more work to do on the many-body side. A more detailed understanding of how errors creep into the calculations will be essential.

Funding: This work was supported by the U.S. Department of Energy, Office of Science, Office of Nuclear Physics, contract no. DEAC02-06CH11357.

Institutional Review Board Statement: Not applicable.

Informed Consent Statement: Not applicable.

Data Availability Statement: Not applicable.

Acknowledgments: I thank my collaborators P. Gysbers, G. Hagen, J. D. Holt, G. R. Jansen, T. D. Morris, P. Navrátil, T. Papenbrock, S. Quaglioni, A. Schwenk, and K. A. Wendt for providing matrix elements of the chiral NN + 3N interactions and axial-vector currents. I also thank T. Miyagi for helpful discussions regarding the KSHELL code and various related scripts, and M. Rho for some enlightening comments.

Conflicts of Interest: The authors declare no conflict of interest.

Appendix A. Table of Gamow–Teller Matrix Elements

Table A1. Matrix elements for the Gamow–Teller transitions plotted in Figures 2 and 3. In the last column, † indicates the lowest 3 states of the listed J^π in the final nucleus are summed in the matrix element, while * indicates that 4 states are summed.

A	Z_i	Z_f	$2J_i$	$2J_f$	$M(GT)_{\text{exp}}$	$\sigma \tau_{\text{bare}}$	$\sigma \tau_{\text{IMSRG}}$	$M(GT)_{\text{th}}$
6	2	3	0	2	2.748	2.995	2.817	2.776
7	4	3	3	3	2.882	3.088	2.889	2.808
7	4	3	3	1	2.678	2.907	2.709	2.639
12	7	6	2	0	1.184	0.830	0.637	0.616
12	7	6	2	2	2.370	1.816	1.728	1.687
15	8	7	1	1	0.889	1.037	1.077	1.035
17	9	8	5	5	3.168	3.681	3.504	3.424
18	9	8	2	0	2.209	2.860	2.483	2.430
19	10	9	1	1	2.273	2.944	2.641	2.540
20	8	9	0	2	1.058	1.419	1.307	1.266
20	11	10	4	2	2.403	2.430	2.208	2.124
24	13	12	8	8	2.886	3.023	2.731	2.639 †
25	13	12	5	5	1.971	2.433	2.273	2.139
26	14	13	0	2	3.055	3.648	3.128	3.006 *
27	11	12	5	3	1.361	1.718	1.435	1.365
27	14	13	5	5	1.688	1.934	1.703	1.630
30	12	13	0	2	1.090	1.488	1.281	1.181
35	15	16	1	1	1.033	1.299	1.060	0.999
37	19	18	3	3	1.169	1.768	1.633	1.565
39	20	19	3	3	1.308	1.967	1.724	1.628
41	21	20	7	7	2.999	4.073	3.733	3.548
42	21	20	14	12	2.497	3.305	3.006	2.836
42	22	21	0	2	2.038	2.713	2.415	2.237
45	22	21	7	7	1.123	1.513	1.362	1.252
45	23	22	7	7	1.801	2.177	1.982	1.844
47	24	23	3	3	0.942	1.190	1.077	0.967
48	25	24	8	8	3.596	4.081	3.494	3.340 *
49	25	24	5	5	1.364	1.768	1.525	1.466
49	25	24	5	7	0.764	0.768	0.656	0.629
100	50	49	0	2	2.870	5.355	3.717	3.471

References

1. Fermi, E. Versuch einer Theorie der β -Strahlen. I. *Z. Phys.* **1934**, *88*, 161–177. [\[CrossRef\]](#)
2. Lee, T.D.; Yang, C.N. Question of Parity Conservation in Weak Interactions. *Phys. Rev.* **1956**, *104*, 254–258. [\[CrossRef\]](#)
3. Wu, C.S.; Ambler, E.; Hayward, R.W.; Hoppes, D.D.; Hudson, R.P. Experimental test of parity conservation in beta decay. *Phys. Rev.* **1957**, *105*, 1413–1415. [\[CrossRef\]](#)
4. Avignone, F.T.; Elliott, S.R.; Engel, J. Double beta decay, Majorana neutrinos, and neutrino mass. *Rev. Mod. Phys.* **2008**, *80*, 481–516. [\[CrossRef\]](#)
5. Holstein, B.R. Precision frontier in semileptonic weak interactions: Theory. *J. Phys. G Nucl. Part. Phys.* **2014**, *41*. [\[CrossRef\]](#)
6. Hardy, J.C.; Towner, I.S. Superaligned $0^+ \rightarrow 0^+$ nuclear β decays: 2014 critical survey, with precise results for V_{ud} and CKM unitarity. *Phys. Rev. C* **2015**, *91*, 025501. [\[CrossRef\]](#)
7. Hayen, L.; Severijns, N.; Bodek, K.; Rozpedzik, D.; Mougeot, X. High precision analytical description of the allowed β spectrum shape. *Rev. Mod. Phys.* **2018**, *90*, 015008. [\[CrossRef\]](#)
8. Epelbaum, E.; Hammer, H.W.; Meißner, U.G. Modern theory of nuclear forces. *Rev. Mod. Phys.* **2009**, *81*, 1773–1825. [\[CrossRef\]](#)
9. Machleidt, R.; Entem, D.R. Chiral effective field theory and nuclear forces. *Phys. Rep.* **2011**, *503*, 1–75. doi:10.1016/j.physrep.2011.02.001. [\[CrossRef\]](#)
10. Hammer, H.W.; König, S.; van Kolck, U. Nuclear effective field theory: Status and perspectives. *Rev. Mod. Phys.* **2020**, *92*, 025004, [\[CrossRef\]](#)
11. Carlson, J.; Gandolfi, S.; Pederiva, F.; Pieper, S.C.; Schiavilla, R.; Schmidt, K.E.E.; Wiringa, R.B.B. Quantum Monte Carlo methods for nuclear physics. *Rev. Mod. Phys.* **2015**, *87*, 1067–1118. [\[CrossRef\]](#)

12. Hagen, G.; Papenbrock, T.; Hjorth-Jensen, M.; Dean, D.J. Coupled-cluster computations of atomic nuclei. *Rep. Prog. Phys.* **2014**, *77*, 096302. [[CrossRef](#)] [[PubMed](#)]
13. Binder, S.; Langhammer, J.; Calci, A.; Roth, R. Ab initio path to heavy nuclei. *Phys. Lett. B* **2014**, *736*, 119. [[CrossRef](#)]
14. Morris, T.D.; Simonis, J.; Stroberg, S.R.; Stumpf, C.; Hagen, G.; Holt, J.D.; Jansen, G.R.; Papenbrock, T.; Roth, R.; Schwenk, A. Structure of the Lightest Tin Isotopes. *Phys. Rev. Lett.* **2018**, *120*, 152503. [[CrossRef](#)]
15. Hergert, H. A Guided Tour of ab initio Nuclear Many-Body Theory. *Front. Phys.* **2020**, *8*, 1–33. [[CrossRef](#)]
16. Somà, V. Self-Consistent Green's Function Theory for Atomic Nuclei. *Front. Phys.* **2020**, *8*, 1–31. [[CrossRef](#)]
17. Lee, D. Recent Progress in Nuclear Lattice Simulations. *Front. Phys.* **2020**, *8*, 1–7. [[CrossRef](#)]
18. van Kolck, U. The Problem of Renormalization of Chiral Nuclear Forces. *Front. Phys.* **2020**, *8*, 79. [[CrossRef](#)]
19. Phillips, D.R. What hath Weinberg wrought? Reflections on what Weinberg's papers on 'Nuclear Forces from Chiral Lagrangians' did and did not accomplish. *arXiv* **2021**, arXiv:2107.03558.
20. Cirigliano, V.; Dekens, W.; de Vries, J.; Hoferichter, M.; Mereghetti, E. Toward Complete Leading-Order Predictions for Neutrinoless Double β Decay. *Phys. Rev. Lett.* **2021**, *126*, 172002. [[CrossRef](#)]
21. Bogner, S.; Furnstahl, R.; Schwenk, A. From low-momentum interactions to nuclear structure. *Prog. Part. Nucl. Phys.* **2010**, *65*, 94–147. [[CrossRef](#)]
22. Furnstahl, R.J.; Hebeler, K. New applications of renormalization group methods in nuclear physics. *Rep. Prog. Phys.* **2013**, *76*, 126301. [[CrossRef](#)]
23. Hergert, H.; Bogner, S.K.; Morris, T.D.; Schwenk, A.; Tsukiyama, K. The In-Medium Similarity Renormalization Group: A Novel Ab Initio Method for Nuclei. *Phys. Rep.* **2016**, *621*, 165–222. [[CrossRef](#)]
24. Hergert, H. In-Medium Similarity Renormalization Group for Closed and Open-Shell Nuclei. *Phys. Scr.* **2017**, *92*, 023002, [[CrossRef](#)]
25. Hergert, H.; Bogner, S.K.; Lietz, J.G.; Morris, T.D.; Novario, S.J.; Parzuchowski, N.M.; Yuan, F. In-Medium Similarity Renormalization Group Approach to the Nuclear Many-Body Problem. In *An Advanced Course in Computational Nuclear Physics*; Hjorth-Jensen, M., Lombardo, M.P., van Kolck, U., Eds.; Springer: Cham, Switzerland, 2017; pp. 477–570. [[CrossRef](#)]
26. Stroberg, S.R.; Bogner, S.K.; Hergert, H.; Holt, J.D. Nonempirical Interactions for the Nuclear Shell Model: An Update. *Annu. Rev. Nucl. Part. Sci.* **2019**, *69*, 307–362. [[CrossRef](#)]
27. Anderson, E.R.; Bogner, S.K.; Furnstahl, R.J.; Perry, R.J. Operator evolution via the similarity renormalization group: The deuteron. *Phys. Rev. C* **2010**, *82*, 054001. [[CrossRef](#)]
28. Schuster, M.D.; Quaglioni, S.; Johnson, C.W.; Jurgenson, E.D.; Navrátil, P. Operator evolution for ab initio theory of light nuclei. *Phys. Rev. C* **2014**, *90*, 011301. [[CrossRef](#)]
29. Parzuchowski, N.M.; Stroberg, S.R.; Navrátil, P.; Hergert, H.; Bogner, S.K. Ab initio electromagnetic observables with the in-medium similarity renormalization group. *Phys. Rev. C* **2017**, *96*, 034324. [[CrossRef](#)]
30. Tropiano, A.J.; Bogner, S.K.; Furnstahl, R.J. Operator evolution from the similarity renormalization group and the Magnus expansion. *Phys. Rev. C* **2020**, *102*, 034005. [[CrossRef](#)]
31. White, S.R. Numerical canonical transformation approach to quantum many-body problems. *J. Chem. Phys.* **2002**, *117*, 7472. [[CrossRef](#)]
32. Stroberg, S.R.; Calci, A.; Hergert, H.; Holt, J.D.; Bogner, S.K.; Roth, R.; Schwenk, A. Nucleus-Dependent Valence-Space Approach to Nuclear Structure. *Phys. Rev. Lett.* **2017**, *118*, 032502. [[CrossRef](#)]
33. Morris, T.D.; Parzuchowski, N.M.; Bogner, S.K. Magnus expansion and in-medium similarity renormalization group. *Phys. Rev. C* **2015**, *92*, 034331. [[CrossRef](#)]
34. Barrett, B.R.; Navrátil, P.; Vary, J.P. Ab initio no core shell model. *Prog. Part. Nucl. Phys.* **2013**, *69*, 131–181. [[CrossRef](#)]
35. Somà, V.; Navrátil, P.; Raimondi, F.; Barbieri, C.; Duguet, T. Novel chiral Hamiltonian and observables in light and medium-mass nuclei. *Phys. Rev. C* **2020**, *101*, 014318. [[CrossRef](#)]
36. Tichai, A.; Roth, R.; Duguet, T. Many-Body Perturbation Theories for Finite Nuclei. *Front. Phys.* **2020**, *8*, 1–29. [[CrossRef](#)]
37. Gysbers, P.; Hagen, G.; Holt, J.D.; Jansen, G.R.; Morris, T.D.; Navrátil, P.; Papenbrock, T.; Quaglioni, S.; Schwenk, A.; Stroberg, S.R.; et al. Discrepancy between experimental and theoretical β -decay rates resolved from first principles. *Nat. Phys.* **2019**, *15*, 428–431. [[CrossRef](#)]
38. Yao, J.M.; Bally, B.; Engel, J.; Wirth, R.; Rodríguez, T.R.; Hergert, H. Ab Initio Treatment of Collective Correlations and the Neutrinoless Double Beta Decay of ^{48}Ca . *Phys. Rev. Lett.* **2020**, *124*, 232501. [[CrossRef](#)]
39. Sun, Z.H.; Morris, T.D.; Hagen, G.; Jansen, G.R.; Papenbrock, T. Shell-model coupled-cluster method for open-shell nuclei. *Phys. Rev. C* **2018**, *98*, 054320. [[CrossRef](#)]
40. Yao, J.M.; Engel, J.; Wang, L.J.; Jiao, C.F.; Hergert, H. Generator-coordinate reference states for spectra and $0\nu\beta\beta$ decay in the in-medium similarity renormalization group. *Phys. Rev. C* **2018**, *98*, 054311. [[CrossRef](#)]
41. Matsubara, H.; Tamii, A.; Nakada, H.; Adachi, T.; Carter, J.; Dozono, M.; Fujita, H.; Fujita, K.; Fujita, Y.; Hatanaka, K.; et al. Nonquenched Isoscalar Spin-1 Excitations in sd-Shell Nuclei. *Phys. Rev. Lett.* **2015**, *115*, 102501. [[CrossRef](#)]
42. Pastore, S.; Pieper, S.C.; Schiavilla, R.; Wiringa, R.B. Quantum Monte Carlo calculations of electromagnetic moments and transitions in $A \leq 9$ nuclei with meson-exchange currents derived from chiral effective field theory. *Phys. Rev. C* **2013**, *87*, 1–15. [[CrossRef](#)]

43. Wilkinson, D.H. Renormalization of the Axial-Vector Coupling Constant in Nuclear β Decay. *Phys. Rev. C* **1973**, *7*, 930–936. [\[CrossRef\]](#)
44. Wilkinson, D. Renormalization of the axial-vector coupling constant in nuclear β -decay (II). *Nucl. Phys. A* **1973**, *209*, 470–484. [\[CrossRef\]](#)
45. Brown, B.A.; Chung, W.; Wildenthal, B.H. Empirical Renormalization of the One-Body Gamow-Teller β -Decay Matrix Elements in the 1s-0d Shell. *Phys. Rev. Lett.* **1978**, *40*, 1631–1635. [\[CrossRef\]](#)
46. Brown, B.; Wildenthal, B. Experimental and theoretical Gamow-Teller beta-decay observables for the sd-shell nuclei. *At. Data Nucl. Data Tables* **1985**, *33*, 347–404. [\[CrossRef\]](#)
47. Chou, W.T.; Warburton, E.K.; Brown, B.A. Gamow-Teller beta-decay rates for $A \leq 18$ nuclei. *Phys. Rev. C* **1993**, *47*, 163–177. [\[CrossRef\]](#) [\[PubMed\]](#)
48. Martínez-Pinedo, G.; Poves, A.; Caurier, E.; Zuker, A.P. Effective g_A in the pf shell. *Phys. Rev. C* **1996**, *53*, R2602. [\[CrossRef\]](#)
49. Rho, M. Quenching of axial-vector coupling constant in β -decay and pion-nucleus optical potential. *Nucl. Phys. Sect. A* **1974**, *231*, 493–503. [\[CrossRef\]](#)
50. Towner, I.S.; Khanna, F.C. Corrections to the single-particle M1 and Gamow-Teller matrix elements. *Nucl. Phys. A* **1983**, *399*, 334–364. [\[CrossRef\]](#)
51. Ericson, M.; Figureau, A.; Thévenet, C. Pionic field and renormalization of the axial coupling constant in nuclei. *Phys. Lett. B* **1973**, *45*, 19–22. [\[CrossRef\]](#)
52. Scherer, S.; Schindler, M.R. *A Primer for Chiral Perturbation Theory*; Lecture Notes in Physics; Springer: Berlin/Heidelberg, Germany, 2012; Volume 830. [\[CrossRef\]](#)
53. Park, T.S.; Marcucci, L.E.; Schiavilla, R.; Viviani, M.; Kievsky, A.; Rosati, S.; Kubodera, K.; Min, D.P.; Rho, M. Parameter-free effective field theory calculation for the solar proton-fusion and hep processes. *Phys. Rev. C* **2003**, *67*, 055206. [\[CrossRef\]](#)
54. Gårdestig, A.; Phillips, D.R. How Low-Energy Weak Reactions Can Constrain Three-Nucleon Forces and the Neutron-Neutron Scattering Length. *Phys. Rev. Lett.* **2006**, *96*, 232301. [\[CrossRef\]](#) [\[PubMed\]](#)
55. Gazit, D.; Quaglioni, S.; Navrátil, P. Three-Nucleon Low-Energy Constants from the Consistency of Interactions and Currents in Chiral Effective Field Theory. *Phys. Rev. Lett.* **2009**, *103*, 102502; Erratum in **2019**, *122*, 029901. [\[CrossRef\]](#) [\[PubMed\]](#)
56. Krebs, H.; Epelbaum, E.; Meißner, U.G.G. Nuclear axial current operators to fourth order in chiral effective field theory. *Ann. Phys.* **2017**, *378*, 317–395. [\[CrossRef\]](#)
57. Park, T.S.; Jung, H.; Min, D.P. In-medium effective axial-vector coupling constant. *Phys. Lett. Sect. B Nucl. Elem. Part. High-Energy Phys.* **1997**, *409*, 26–32. [\[CrossRef\]](#)
58. Menéndez, J.; Gazit, D.; Schwenk, A. Chiral Two-Body Currents in Nuclei: Gamow-Teller Transitions and Neutrinoless Double-Beta Decay. *Phys. Rev. Lett.* **2011**, *107*, 062501. [\[CrossRef\]](#)
59. Ekström, A.; Jansen, G.R.; Wendt, K.A.; Hagen, G.; Papenbrock, T.; Bacca, S.; Carlsson, B.; Gazit, D. Effects of three-nucleon forces and two-body currents on Gamow-Teller strengths. *Phys. Rev. Lett.* **2014**, *113*, 262504. [\[CrossRef\]](#)
60. Holt, J.W.; Brown, G.E.; Kuo, T.T.S.; Holt, J.D.; Machleidt, R. Shell model description of the ^{14}C dating β decay with Brown-Rho-scaled NN interactions. *Phys. Rev. Lett.* **2008**, *100*, 1–4. [\[CrossRef\]](#)
61. Maris, P.; Vary, J.P.; Navrátil, P.; Ormand, W.E.; Nam, H.; Dean, D.J. Origin of the Anomalous Long Lifetime of ^{14}C . *Phys. Rev. Lett.* **2011**, *106*, 202502. [\[CrossRef\]](#)
62. Pastore, S.; Baroni, A.; Carlson, J.; Gandolfi, S.; Pieper, S.C.; Schiavilla, R.; Wiringa, R.B. Quantum Monte Carlo calculations of weak transitions in $A = 6$ –10 nuclei. *Phys. Rev. C* **2018**, *97*, 022501. [\[CrossRef\]](#)
63. Faestermann, T.; Schneider, R.; Stolz, A.; Sümmerer, K.; Wafers, E.; Friese, J.; Geissel, H.; Hellström, M.; Kienle, P.; Körner, H.J.; et al. Decay studies of $N \approx Z$ nuclei from 75Sr to 102Sn. *Eur. Phys. J. A* **2002**, *15*, 185–188. [\[CrossRef\]](#)
64. Batist, L.; Górska, M.; Grawe, H.; Janas, Z.; Kavatsyuk, M.; Karny, M.; Kirchner, R.; la Commara, M.; Mukha, I.; Plochocki, A.; et al. Systematics of Gamow-Teller beta decay "Southeast" of ^{100}Sn . *Eur. Phys. J. A* **2010**, *46*, 45–53. [\[CrossRef\]](#)
65. Hinke, C.B.; Böhmer, M.; Boutachkov, P.; Faestermann, T.; Geissel, H.; Gerl, J.; Gernhäuser, R.; Górska, M.; Gottardo, A.; Grawe, H.; et al. Superaligned Gamow-Teller decay of the doubly magic nucleus ^{100}Sn . *Nature* **2012**, *486*, 341–345. [\[CrossRef\]](#)
66. Lubos, D.; Park, J.; Faestermann, T.; Gernhäuser, R.; Krücken, R.; Lewitowicz, M.; Nishimura, S.; Sakurai, H.; Ahn, D.S.; Baba, H.; et al. Improved Value for the Gamow-Teller Strength of the ^{100}Sn Beta Decay. *Phys. Rev. Lett.* **2019**, *122*, 222502. [\[CrossRef\]](#)
67. Stroberg, S.R. Imsrg++ Code. Available online: <https://github.com/ragnarstroberg/imsrg> (accessed on 27 October 2021).
68. Brown, B.A.; Rae, W.D.M. The Shell-Model Code NuShellX@MSU. *Nucl. Data Sheets* **2014**, *120*, 115–118. [\[CrossRef\]](#)
69. Stroberg, S.R. Nutbar Code. Available online: <https://github.com/ragnarstroberg/nutbar> (accessed on 27 October 2021).
70. Shimizu, N. Nuclear shell-model code for massive parallel computation, "KSHELL". *arXiv* **2013**, arXiv:1310.5431.
71. Bogner, S.K.; Kuo, T.T.S.; Schwenk, A. Model-independent low momentum nucleon interaction from phase shift equivalence. *Phys. Rep.* **2003**, *386*, 1–27. [\[CrossRef\]](#)
72. Cohen, S.; Kurath, D. Effective interactions for the 1p shell. *Nucl. Phys.* **1965**, *73*, 1–24. [\[CrossRef\]](#)
73. Engel, J.; Menéndez, J. Status and Future of Nuclear Matrix Elements for Neutrinoless Double-Beta Decay: A Review. *Rep. Prog. Phys.* **2017**, *80*, 046301. [\[CrossRef\]](#) [\[PubMed\]](#)
74. Seng, C.Y.; Gorchtein, M.; Ramsey-Musolf, M.J. Dispersive evaluation of the inner radiative correction in neutron and nuclear β decay. *Phys. Rev. D* **2019**, *100*, 13001. [\[CrossRef\]](#)

75. Miller, G.A.; Schwenk, A. Isospin-symmetry-breaking corrections to superallowed Fermi β decay: Radial excitations. *Phys. Rev. C* **2009**, *80*, 064319. [[CrossRef](#)]
76. Hebeler, K.; Bogner, S.K.; Furnstahl, R.J.; Nogga, A.; Schwenk, A. Improved nuclear matter calculations from chiral low-momentum interactions. *Phys. Rev. C* **2011**, *83*, 031301. [[CrossRef](#)]
77. Tichai, A.; Müller, J.; Vobig, K.; Roth, R. Natural orbitals for ab initio no-core shell model calculations. *Phys. Rev. C Nucl. Phys.* **2019**, *99*, 034321. [[CrossRef](#)]
78. Hoppe, J.; Tichai, A.; Heinz, M.; Hebeler, K.; Schwenk, A. Natural orbitals for many-body expansion methods. *Phys. Rev. C* **2021**, *103*, 014321. [[CrossRef](#)]
79. Furnstahl, R.J.; Hagen, G.; Papenbrock, T. Corrections to nuclear energies and radii in finite oscillator spaces. *Phys. Rev. C* **2012**, *86*, 031301. [[CrossRef](#)]
80. Furnstahl, R.J.; Phillips, D.R.; Wesolowski, S. A recipe for EFT uncertainty quantification in nuclear physics. *J. Phys. G Nucl. Part. Phys.* **2014**, *42*, 034028. [[CrossRef](#)]
81. Hagen, G. (Oak Ridge National Laboratory). Private communication, 2019.
82. Belley, A.; Payne, C.G.; Stroberg, S.R.; Miyagi, T.; Holt, J.D. Ab Initio Neutrinoless Double-Beta Decay Matrix Elements for Ca 48, Ge 76, and Se 82. *Phys. Rev. Lett.* **2021**, *126*, 042502. [[CrossRef](#)]
83. Yao, J.M.; Belley, A.; Wirth, R.; Miyagi, T.; Payne, C.G.; Stroberg, S.R.; Hergert, H.; Holt, J.D. Ab initio benchmarks of neutrinoless double- β decay in light nuclei with a chiral Hamiltonian. *Phys. Rev. C* **2021**, *103*, 014315. [[CrossRef](#)]
84. Hagen, G.; Papenbrock, T.; Hjorth-Jensen, M. Ab initio computation of the F17 proton halo state and resonances in $A = 17$ nuclei. *Phys. Rev. Lett.* **2010**, *104*, 5–8. [[CrossRef](#)]
85. Heinz, M.; Tichai, A.; Hoppe, J.; Hebeler, K.; Schwenk, A. In-medium similarity renormalization group with three-body operators. *Phys. Rev. C* **2021**, *103*, 044318. [[CrossRef](#)]
86. Simonis, J.; Stroberg, S.R.; Hebeler, K.; Holt, J.D.; Schwenk, A. Saturation with chiral interactions and consequences for finite nuclei. *Phys. Rev. C* **2017**, *96*, 014303. [[CrossRef](#)]
87. Taniuchi, R.; Santamaria, C.; Doornenbal, P.; Obertelli, A.; Yoneda, K.; Authalet, G.; Baba, H.; Calvet, D.; Château, F.; Corsi, A.; et al. ^{78}Ni revealed as a doubly magic stronghold against nuclear deformation. *Nature* **2019**, *569*, 53–58. [[CrossRef](#)]
88. Stroberg, S.R.; Holt, J.D.; Schwenk, A.; Simonis, J. Ab initio Limits of Atomic Nuclei. *Phys. Rev. Lett.* **2021**, *126*, 022501. [[CrossRef](#)] [[PubMed](#)]
89. Hagen, G.; Jansen, G.R.; Papenbrock, T. Structure of ^{78}Ni from First-Principles Computations. *Phys. Rev. Lett.* **2016**, *117*, 172501. [[CrossRef](#)]
90. Gaarde, C. Gamow-Teller and M1 resonances. *Nucl. Phys. Sect. A* **1983**, *396*, 127–144. [[CrossRef](#)]
91. Cheon, T.; Takayanagi, K. Isospin-Dependent Effective Interaction in Nucleon-Nucleus Scattering. *Phys. Rev. Lett.* **1992**, *68*, 1291. [[CrossRef](#)] [[PubMed](#)]
92. Zegers, R.G.T.; Akimune, H.; Austin, S.M.; Bazin, D.; Berg, A.M.D.; Berg, G.P.; Brown, B.A.; Brown, J.; Cole, A.L.; Daito, I.; et al. The (t, He^3) and (He^3, t) reactions as probes of Gamow-Teller strength. *Phys. Rev. C Nucl. Phys.* **2006**, *74*, 1–15. [[CrossRef](#)]